Materials Innovations

HΣXA Publishers

Computational Materials Science | Research Article | http://doi.org/10.54738/MI.2022.2402

# Ab-initio Investigation of Structural, Optoelectronic, and Magnetic Properties of $SmAlO_3$

**Nazia Erum[1]*, Muhammad Azhar Iqbal[2], Sadia Sagar[1], Sher Nawaz[1]**

**1** Physics Department, The University of Lahore, New Campus, Defense Road, 54000, Lahore, Pakistan
**2** Department of Physics, University of the Punjab, Quaid e Azam Campus, Lahore, 54000, Pakistan



**Received:** 11 February 2022
**Accepted:** 13 March 2022
**Published:** 30 April 2022

**Citation:** Erum N, Azhar Iqbal M, Sagar S, Nawaz S (**2022**) Ab-initio Investigation of Structural, Optoelectronic, and Magnetic Properties of $SmAlO_3$. *Materials Innovations 2* (4), 123-131.

***Correspondence**: (Nazia Erum)
nazia.erum@phys.uol.edu.pk



Published By Hexa Publishers

**ISSN**
Electronic: 2790-1963

*The cubic perovskites have attained great importance in magneto-electronic storage devices due to their electromagnetic nature and because of their direct band-gap. The cubic perovskites' structural, electronic, optical, and magnetic characteristics were investigated using Density Functional Theory (DFT), using Wein2k-code with the Full Potential Linearized Augmented Plane Wave (FP-LAPW) method. In Kohn-sham equations, the Generalized Gradient Approximation (GGA) has been used as an exchange-correlation function. Investigated structural properties by analytical methods as well as DFT establish to be similar in comparison with the results of experimental data. The optimizations of the stable magnetic phase authenticate the low-temperature experimental observations. The optical spectra also deliver various linear optical parameters. So the current investigation signifies a valuable approach to analyze the comprehensive data about structural, magneto-electronic, and optical properties that can create a prospect to comprehend profuse physical occurrences of $SmAlO_3$. In addition to it, authorize material scientists to implement the material for valuable applications.*

**Keywords:** Opto-Electronic properties, Magnetic properties, ab-initio method

## INTRODUCTION

In a variety of optoelectronic and photonic device applications, perovskite materials have been reported as the most attractive and efficient reduced energy materials. Perovski's invention of calcium titanate (CaTiO3) in 1839 was regarded as the beginning of perovskite, and minerals with about the same crystal structure as CaTiO3 were referred to as perovskite materials (structure). Perovskite materials have the chemical formula ABX3, in which A and B are cations, with A usually bigger than B, and X is the anion, which is usually oxides or halogens. Perovskite materials have piqued interest in optoelectronic and photovoltaic technology due to their unusual physical properties, their absorption coefficient is high, and they have long-range bipolar charge transfer, and low exciting-binding energy, high dielectric constant, and ferroelectric characteristics, among other things. Miyasaka et al.[1] accomplished the first success in methyl ammonium halide ($MAX_3$) perovskites by using $MAX_3$ perovskites as light-absorbing materials in a photovoltaic device. They are attractive materials for solar applications because of their high absorption coefficient, long diffusion length, superior charge-transport characteristics, low nonradioactive rad-

iation, and solution process ability[2–4]. Thanks to remarkable advancements in perovskite thin film research, the efficiency of solar systems, there has been a rise in the use of perovskite materials. From 3.8 percent to 22.1 percent[5] in just 6 years. LEDs[6–8], photodetectors, nano lasers, and waveguides all utilize perovskite materials. In perovskite thin film based optoelectronic and photovoltaic systems, the quality of the perovskite thin film (morphology, grain size, homogeneity, coverage.

The perovskite films were deposited via spin coating of perovskite solutions, successive deposit of solutions, and heat evaporation. Leading to a better photovoltaic performance, the devices must be fabricated and measured in a controlled (inert) environment to avoid material degradation under ambient circumstances. The endeavor to enhance the efficiency and environmental perovskite stability-based electronics included the development of new device topologies as well as the synthesis of novel stable materials[9,10].

The discovery of low-dimensional (LD) perovskite materials, as well as research into their characteristics for photonic and optoelectronic device applications, has resurfaced recently. LD materials and nanocrystals are materials with at least one dimension in the nanoscale (1–100 nm) (NCs). The optical and electrical properties of LD perovskite materials can be adjusted, as well as mechanical flexibility, thanks to quantum-sized effects, which is getting more interest in Optoelectronic devices and semiconductor materials. The optoelectronic properties of LD perovskites are greatly improved by reducing the dimensionality of bulk perovskite materials. For a long time, LEDs, photovoltaics, photodetectors, and lasing uses have all been around[11–13].

These investigations' preliminary findings revealed the materials' potential in photonics and optoelectronics. The device's performance and stability can yet be improved, which will require a detailed examination of the materials' qualities. An indefinite number of two-dimensional slabs are separated by an element with the structure $ABX_3$ in a layered perovskite structure. Hybrid halide perovskites have emerged as a promising new class of materials for flexible solar applications, owing to their ability to be produced at low temperatures and hence coated on plastic substrates[14]. Perovskite hardens from a liquid with a silica activity on or below the titanite to perovskite + silica buffer in basic and alkaline igneous rocks, showing precipitation from a liquid with a silica activity on or below the titanite. Low silica activity olivine melilites (1–9%), kimberlites (1–%), foidites, clinopyroxenites, and carbonatites all include perovskite. A scanning electron microscopes back-scattered electron facility may clearly demonstrate oscillatory zonation in perovskite created in igneous environments. When carbonates undergo contact metamorphism, perovskite is manufactured, and it is most typically encountered as Ce- or Nb-bearing forms. The lower mantle is anticipated to contain a substantial amount of $MgSiO_3$ perovskite, with CaSiO3 perovskite being the most important[15,16].

Perovskite (orthorhombic $CaTiO_3$) is present near the Earth's surface, however, as pressure and temperature increase, some Ca is replaced by Fe, resulting in the formation of $CaFe_3Ti4O_{12}$. Ti is replaced by Si in the higher mantle, and cubic $CaSiO_3$ is discovered. At lower mantle pressures, $MgSiO_3$ perovskite is projected to form, with a transition to an orthorhombic" post-perovskite" phase near the core-mantle boundary. Perovskite has been found in meteorites and in carbonaceous chondrites' Ca-Al-rich refractory inclusions (CAI). It is one of the primitive solar nebula's early condensates, thought to have formed within the first 1 Ma of the solar nebula's existence[17].

Chemicals and stoichiometry are used by the perovskite structure to taken in light. Researchers still are puzzled as to why the positive and negative charges created by light excitation in these cells reach their electrodes so efficiently. The high rate of advancement, on the other hand, motivated PV scientists in industry and academia who worked with other types of cells to move to perovskites or take the initiative. Because of its widespread availability in nature, perovskite has caught the interest of material scientists. In the recent decade, perovskite solar cells (PSC) have seen a lot of success in photovoltaic applications. From 3.8 percent in 2009 to 25.6 percent in 2021, the power conversion efficiency (PCE) has increased dramatically. The physical and chemical characteristics of rare earth aluminates, in instance, can nucleate to produce perovskite-like structures linked to their crystallographic characteristics[18]. Due to its good dielectric and hardness qualities, high melting point, and refractive index, Samarium Aluminate ($SmA1O_3$) has drawn a lot of attention in this field. Perovskite-structured ceramics are gaining popularity in material science because they have a wide range of applications in domains like optics, photovoltaics, electronics, magnetics, catalysis, sensing, and more[19].

In this manuscript, the structural, electrical, optical, and magnetic properties of $SmAlO_3$ are calculated. The optical characteristics of $SmAlO_3$ will be evaluated using optical conductivity, absorption coefficient, energy loss function, reflectivity, refractive index, extinction coefficient, and dielectric constant. The density of States (DOS), Electron Density, and Energy Band Gap will be used to analyze the electronic characteristics of $SmAlO_3$ . In terms of structural aspects, the samarium atoms are found at the corners of the unit cell. The aluminum atom is found in the body center of the unit cell, whereas the red-colored oxy-

gen atoms are found in the face Centre. Researchers at Oxford University in the United Kingdom revealed that perovskite can be used as a thin-film solar cell alternative[12]. The structural, electrical, and magnetic features of the ground state are explored in light of their sophisticated technological applications.

## COMPUTATIONAL DETAILS

The calculations were carried out using the FP-LAPW method, which is one of the most efficient methods for calculating the ground state properties of materials, as implemented in the WIEN2k code. For the exchange and correlation potentials, Generalized Gradient Approximation (GGA) and GGA+U approximations were utilized, and the GGA plus Trans-Blaha modified Becke–Johnson (TB-mBJ) potential was also used for effective representation of the band gap, followed by the Spin Orbit Coupling (SOC), accordingly. Additionally, optimizations of each unit cell are performed to obtain ground state structural parameters by fitting Birch-Murnaghan equation of state[20–22]. The details of spin-dependent FP-LAPW method, its computational information regarding WIEN2K package, used in this work can be found in Refs.[23]. In WIEN2K package, valence electrons treatment are done semi-relativistically although, core electrons are treated fully relativistically[24]. But for convergence in basis size a cut-off value of $RMTK_{max}$ = 8.0 is used. Additionally, to achieve well-converged optimum results of structural properties, 56 K point integration in brillouin zone (BZ) is done with modified form of tetrahedron method. Conversely, for calculating electronic, as well as magneto-optic properties a denser mesh of 2000 K-points are used. The self-consistent converged calculation are achieved when charge total as well as energy is stable within $10^{-6}$ eV correspondingly.

By following a few basic procedures and utilizing the calculations made by the SCF cycle, we obtained an electron density graph in the execution menu. There are two output options: a 3D plot and a 2D contour plot. It can be used to describe how electrons are distributed in different materials. The density of states of $SmAlO_3$ are found out individually using GGA. Electrons in the Al-2p and O-2p states, which are up to 1 eV below the Fermi level, $E_F$, make up the core areas. The contribution of the O-2p states in the valence region is greater than that of the Al-2p states. The peaks owing to the Sm-4f states in the spin-up configuration for the GGA and GGA+U approximations are positioned at 1, 0.5, and 0.25 eV. The band gap for $SmAlO_3$ is calculated. Band structures of SmAlO3 show that when the material is spun up, the Fermi level crosses the valence band, showing that it is a semiconductor. The difference in band gap energy between the conduction and valence bands is almost 2eV, which agrees with experimental observations and indicates that the material is a semiconductor. Using wein2k, FPLAPW and GGA further properties like optical, electronic and magnetic properties are found.

## RESULTS AND DISCUSSION

Different properties of $SmAlO_3$ were found in this section using different methods.

### Structural Properties

This illustration shows a single perovskite cell with Samarium atoms at the corners, Aluminum atoms at the cell's body centered location, and red coloured Oxygen atoms at the unit cell's face centered region as shown in figure.

The experimental lattice parameters were being used[13]. In Figure 2, the estimated equilibrium lattice constants a and c (in A), volume vs relative energy curve, bulk modulus B (in GPa), and its pressure derivative (BP) for the $SmAlO_3$ compound are displayed. Lattice parameters derived with GGA are overstated by 1–2% when compared to experimental values, as expected.[14]

### Electronic Properties

The nature of the chemical bond is analyzed with the help of contour maps of the electron density. The contour plots of electron density can play a significant role in describing the nature of chemical bonding in solids[20]. By following a few basic procedures and utilizing the calculations made by the SCF cycle, we may obtain an electron density graph in the execution menu. There are two output options: a 3D plot and a 2D contour plot. It can be used to describe how electrons are distributed in different materials. We choose to plot two-dimensional electronic charge densities as shown in Figure 3. Here the distribution of charges between the Sm cation and O anion is likely to be spherical for $SmAlO_3$, which indicates the prevalent nature of the ionic bond in this compound. While, due to large difference of electronegativity, the charge transfer in the octahedrals varies accordingly and the chemical bond is formed between two chemical elements with larger electronegativity difference, and the bonding tends towards more ionic in nature.

When determining band structure, we must do a large number of symmetry operations in order to acquire very exact and precise results. We must employ a large number of K-points, such as 1000 or more, to start and run the SCF- Cycle.

$$E_g = -E_{VBM}$$

Figure 4(b) depicts the band structures for spin up and spin down, and the band gap energy is represented by the equation 1. The Fermi level is set at 0 eV. For $SmAlO_3$, the energy gap is absent for the spin up channel, thus indicating their metallic behavior in the spin-up channel. On the other hand, for spin down channel energy gaps is

*Table 1. The calculated equilibrium lattice parameters a, b and c (in °A).*

| Lattice parameters | Calculated | Ref. 15 | Ref. 47 | Ref. 6 |
|---|---|---|---|---|
| a (°A) | 5.38 | 5.29 | 5.267 | 5.28 |
| b (°A) | 5.37 | 5.29 | 5.277 | 5.26 |
| c (°A) | 7.59 | 7.47 | 7.444 | 7.4 |

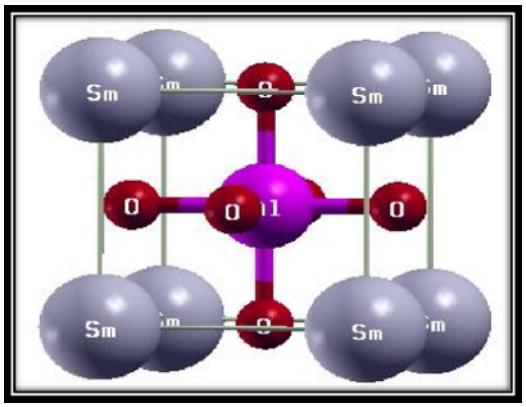


*Figure 1. The cubic structure of $SmAlO_3$.*

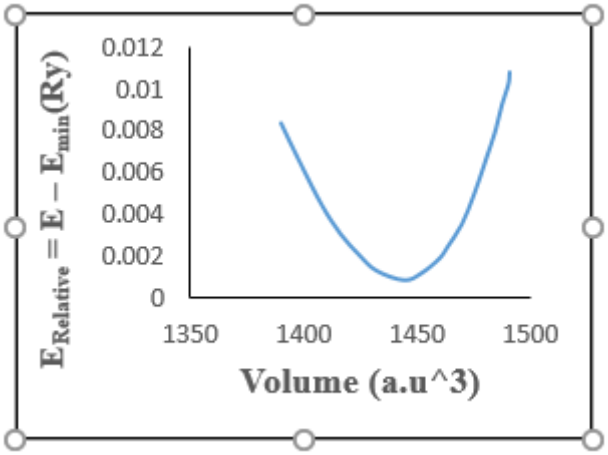


*Figure 2. The computed relative energies (Ry) vs volume.*

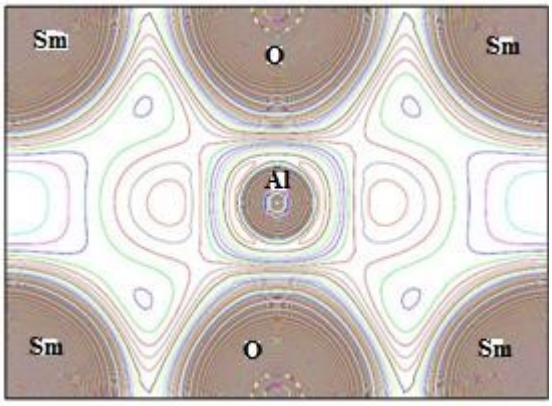


*Figure 3. Calculated total two-dimensional electronic charge densities.*

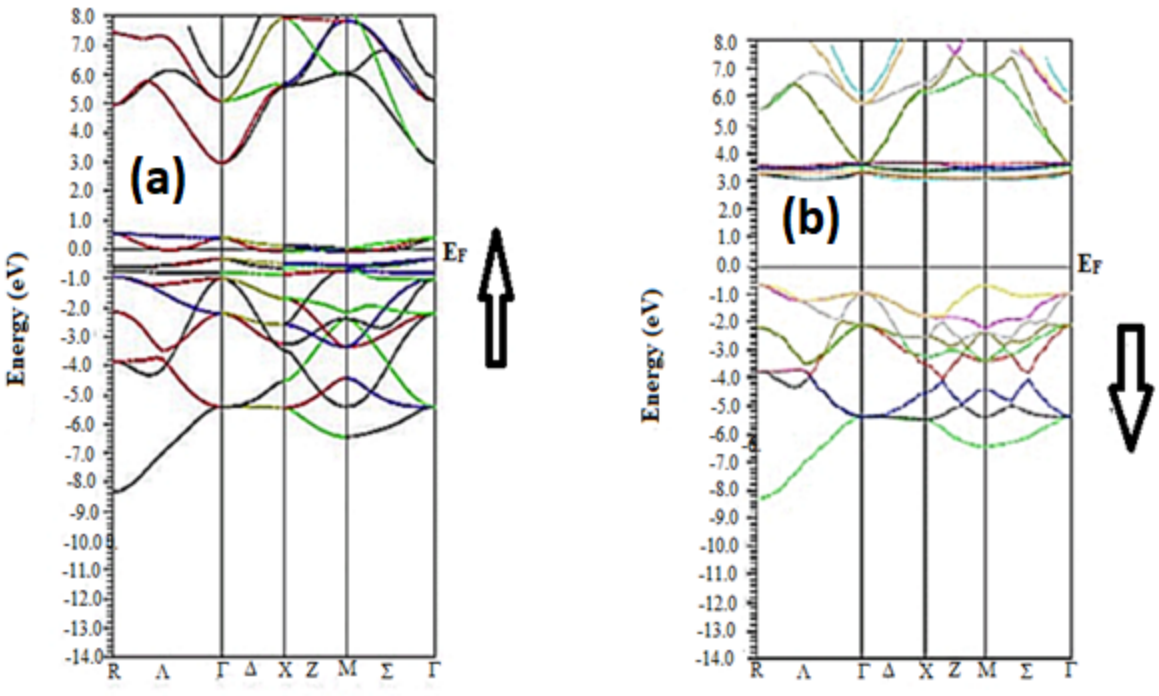


*Figure 4. (a-b):Band Gap (Up and Down) structures of $SmAlO_3$.*

present and the difference between the conduction as well as valence bands is almost 2 eV so it can be concluded that $SmAlO_3$ compound is a semiconductor.

The nature of the electronic band structure can be precisely analyzed with the help of the partial and total density of states (DOS). The calculated results of the total and partial DOS indicate the wide electronic dispersions. Peaks in the density of states can be efficiently analyzed by dividing the band diagram into three main regions, namely the conduction band region, the valence band region and the bands situated at or near the Fermi level energy ($E_F$)[19–21]. As a result, $SmAlO_3$ has magnetic moments and is a magnetic material. The GGA results in Figure 5(a-d) indicate that the $SmAlO_3$ compound is half metallic, but the DOS contribution has indeed been reduced marginally. The partial and total densities of states (DOSs) for $SmAlO_3$, Sm-4f, Al-2p, and O-total (2s+2p) in the GGA, GGA+U (U = 0.51 Ry), and O-total (2s+2p) in the GGA, GGA+U (U = 0.51 Ry), Approximations mBJ+U and mBJ+U+SOC, respectively, are shown in the GGA. The DOS profiles for these four approximations are nearly comparable in terms of quality.

## Optical Properties

This section is devoted to explore the optical properties of $SmAlO_3$ compounds to the applied field of electromagnetic radiation with GGA approximation[22,23]. The optical properties are calculated using complex form of dielectric function denoted as $\varepsilon(\omega)$. The details are mentioned in the following relation[24]:

$$\varepsilon(\omega) = \varepsilon_1(\omega) + i\varepsilon_2(\omega) \qquad (2)$$

These properties includes the energy loss function L($\omega$), absorption coefficient $\alpha(\omega)$, optical conductivity $\sigma(\omega)$, refractive index n($\omega$), reflectivity R ($\omega$), and the effective number of electrons ($n_{eff}$) by sum rules along xx-direction are presented in Figure 6(a-h).

In the spectrum of real part of dielectric function $\varepsilon_1(\omega)$, the zero frequency limit $\varepsilon_1(0)$ which provides static dielectric constant (as shown in figure) in the zero frequency limits. In Figure 6(a) Real component of the dielectric constant shows peak values at 1.69 eV, 6.26 eV, 6.70 eV, 14.76, and 23.72 eV. When the energy value of 26.19 eV rises, the dielectric constant rises slightly. Our analysis of corresponding $\varepsilon_2$ ($\omega$) peaks trail the similar pattern of the density of states (DOS) and band structure of investigated compounds But for the Imaginary part peak values are observed at energy levels of 2.03 eV, 7.47 eV, 14.90 eV, and 24.03 eV, as shown in the accompanying graph in Figure 6(b). The purpose of optical conductivity $\sigma(\omega)$ is to describe the phenomenon of electron conduction due to applied electromagnetic field. The phenomenon of conductivity originates at about 2eV from small ascending peak which finally reaches to its divergent sharp maxima at about 12 eV. The purpose of optical conduc-

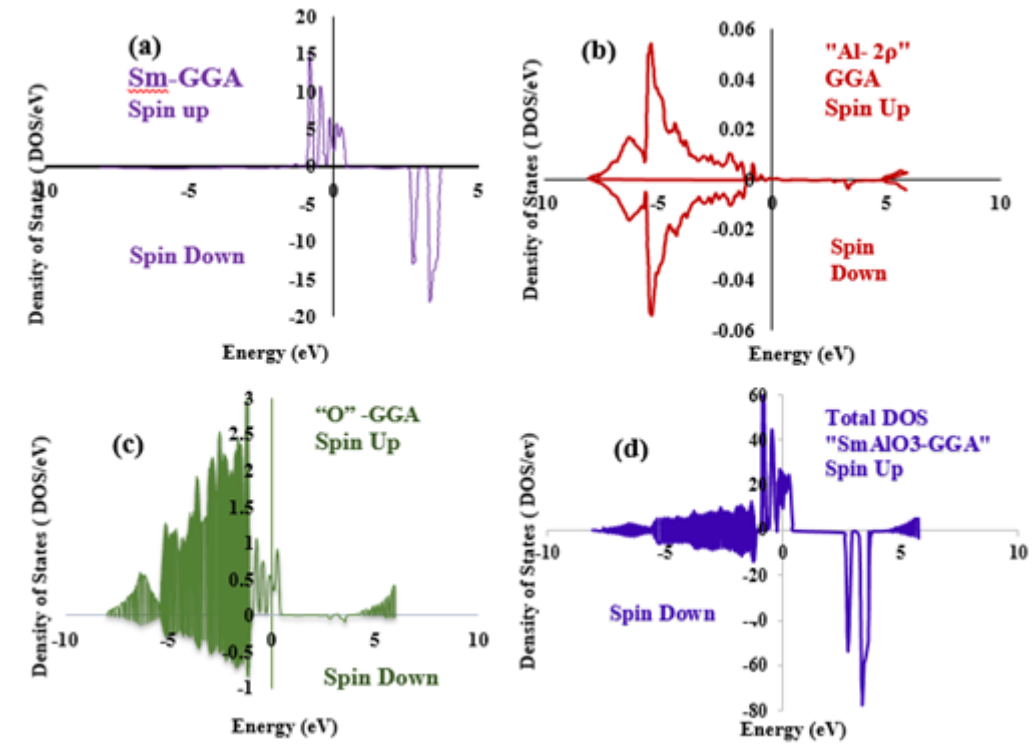


*Figure 5. (a-d): Spin-dependent total and partial density of states for $SmAlO_3$.*

tivity $\sigma(\omega)$ is to describe the phenomenon of electron conduction due to applied electromagnetic field. The phenomenon of conductivity originates at about 5eV from small ascending peak which finally reaches to its divergent sharp maxima at about 19 eV. The optical conductivity of SmAlO3 is summarized in Figure 6(c), where we can see that the real ($\sigma$) component increases with increasing photon energy, with a maximum peak near 8.5 eV. However, when photon energy increases, the imaginary ($\sigma$) part decreases and becomes negative, generating a valley around 7.3 eV of energy and subsequently a sudden climb towards zero. Figure 6(d) When it comes to energy, there is no absorption.

From the plot of absorption coefficient it can be inferred that compounds initiates absorbing electromagnetic radiation at about value of 2.25 eV as displayed in Figure 6(d). This particular energy (threshold point) is exactly in accordance with trend of bandgaps and $\sigma$ ($\omega$) plots. However, these compounds start absorption within range of 8-12 eV and noticeable peak is detected at about 20 eV. The absorption increases until the energy reaches about 10.3ev, as can be observed. After that, absorption tends to slow down. Figure 6(e) Energy losses at low frequencies are insignificant, as shown in Figure 6(e). At energy values of 6.44eV, 12.10eV, and 20.55eV, the energy loss is minimal. The energy loss starts at a high of 30.04 eV and quickly drops to 39.60 eV. The energy loss is virtually zero after 40.33 eV.

The peak changes toward smaller energy losses as the amount of energy increases.

The reflectivity spectrum has a qualitative tendency that is comparable to those obtained by Zhu et al. in the range of 1060–1068 nm at room temperature, however the reflectivity in this calculation is lower. The minimal reflectivity at 1.13 eV (= 1.097 m) (which is comparable to the minima at 1.075 m in the experimental result) is shown in the inset in Figure 6(f), which is the same as reported in Zhu et al.[24]. Figure 6(g) shows that refractive index reaches a maximum of 6.5 at 0 eV. As the amount of energy grows, the value decreases. At about 7.4 ev, there is a modest increase in refractive index. The extinction coefficient graph as in Figure 6(h) shows the highest peaks at 2.01 eV, 7.87 eV, 8.65 eV, 9.79 eV, 15.15 eV, 24.74 eV, and 26.27 eV. Valley spots are found at 1.32 eV, 5.01 eV, 13.23 eV, and 22.18 eV, with the value dropping after that.

## Magnetic Properties

In condensed matter, magnetism arises due to the combination of individual atoms according to the crystal structure of solids[21–23]. The concept of magnetism exists due to partially filled electron shells[24]. To study the magnetic behavior of the $SmAlO_3$ compound we calculate the total, local, and intersti-

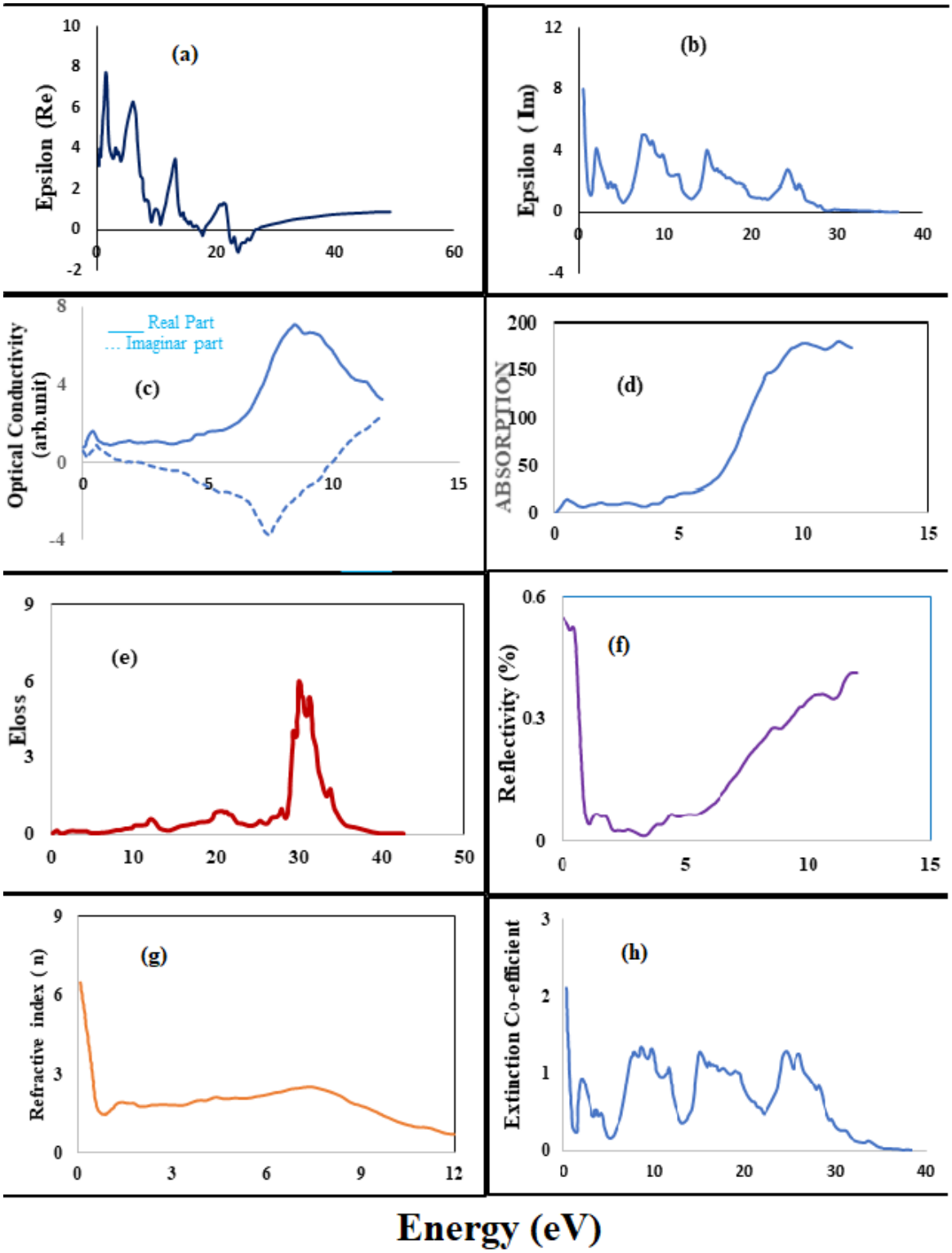


*Figure 6. (a) Real partof dielectric function (b) Imaginary part of dielectric function (c) CalculatedReal and imaginary parts of Optical conductivity (σ) (d) Absorption curve(e) Energy loss function (f) Reflectivity (g) Refractive index (n) (h)Extinction coefficient of $SmAlO_3$.*

*Table 2. The calculatedmagnetic moments in Bohr magnetron uB of several sites of orthorhombic $SmAlO_3$.*

| | |
|---|---|
| Total Megnatic Moment *($\mu Btotal$)* | 4.99981 |
| Magnetic Moment Interstitial *($\mu B_{intersl}$)* | 0.06858 |
| Magnetic Moment Samarium ($\mu B_{Sm}$) | 5.18381 |
| Magnetic Moment Aluminum *($\mu B_{Al}$)* | 0.00185 |
| Magnetic Moment Oxygen *($\mu B_{O}$)* | - 0.08481 |

tial magnetic moments as presented in Table 2. In $SmAlO_3$, the exchange interaction between the rare earth metal and the nonmagnetic ion O gives rise to its magnetic properties. However, the positive magnetic moments of interstitial sites and o atoms reveal they are parallel to magnetic moments of Aluminum. The total magnetic moment of $SmAlO_3$ compound is 4.99981. Furthermore, the integer value of the total magnetic moment a reveals half-metallic nature in this compound which is in accordance with the Slater-Pauling rule [25]. These prominent characteristics make these compounds suitable for various applications.

## CONCLUSIONS

Finally, we used FPLAPW.GGA and Wein2k undertake a comprehensive computation on the structural, electrical, optical, and magnetic properties of $SmAlO_3$. Structural properties are calculated by giving the values of the number of atoms, lattice type, space group, symbols of atoms of our compound, their locations, their respective atomic numbers, and RMT values, using the WIEN2k algorithm. The optimization curve has been plotted between energy and volume by using the calculated values of energy and volume. Electronic properties such as band gap plots, Density of States (DOS), and Electron density plots are also calculated. The results of electronic properties show that the $SmAlO_3$ compound is half metallic in nature. Optical properties are also calculated in detail. For the calculation of these optical properties, we defined dielectric function ($\varepsilon$). Using these optical properties calculations, we determined optical conductivity, absorption coefficient, reflectivity, dielectric constant, and refractivity and plotted them. The optical conductivity of SmAlO3 is summarized where we can see that the real ($\sigma$) component increases with increasing photon energy, with a maximum peak near 8.5 eV. However, when photon energy increases, the imaginary ($\sigma$) part decreases and becomes negative, generating a valley around 7.3 eV of energy and subsequently a sudden climb towards zero. The absorption continues to rise as the energy increases. The absorption increases until the energy reach about 10.3ev, as can be observed. After that, absorption tends to slow down. Energy losses at low frequencies are insignificant. At energy values of 6.44 eV, 12.10 eV, and 20.55eV, the energy loss is minimal. The energy loss starts to reach at a high of 30.04 eV and quickly drops to 39.60 eV. The energy loss is virtually zero after 40.33 eV. The peak changes toward smaller energy losses as the number of energy increases. The absorption continues to rise as the energy increases. The absorption increases until the energy reach about 10.3eV, as can be observed. After that, absorption tends to slow down. Energy losses at low frequencies are insignificant. At energy values of 6.44eV, 12.10eV, and 20.55eV, the energy loss is minimal. The energy loss starts at a high of 30.04 eV and quickly drops to 39.60 eV. The energy loss is virtually zero after 40.33 eV. The peak changes toward smaller energy losses as the number of energy increases. The same is the case reflectivity, the minimal reflectivity at 1.13 eV (= 1.097 m) (which is comparable to the minima at 1.075 m in the experimental result) can be seen in the graph, which is the same as reported by Zhu et al. The extinction coefficient graph shows the highest peaks at 2.01 eV, 7.87 eV, 8.65 eV, 9.79 eV, 15.15 eV, 24.74 eV, and 26.27 eV. Valley spots are found at 1.32 eV, 5.01 eV, 13.23 eV, and 22.18 eV, with the value dropping after that. At last magnetic properties of $SmAlO_3$ are calculated. The magnetic characteristics of $SmAlO_3$ are due to the exchange interaction between the rare earth metal and the nonmagnetic ion O. The computed magnetic moments per unit cell for the interstitial, local, and total magnetic moments.

## References


1) Erum, N.; Iqbal, M. A.; Sagar, S.; Nawaz, M. Insight into the Opto-electronic Properties of AgGas2 under Axial Strain via ab-initio Calculations. *Materials Innovations* **2021**, *01* (01), 34–45, DOI: 10.54738/MI.2021.1101, available at http://doi.org/10.54738/MI.2021.1101.
2) Kojima, A.; Teshima, K.; Shirai, Y.; Miyasaka, T. Organometal Halide Perovskites as Visible-Light Sensitizers for Photovoltaic Cells. *Journal of the American Chemical Society* **2009**, *131* (17), 6050–6051, DOI: 10.1021/ja809598r, available at https://doi.org/10.1021/ja809598r.
3) Yang, W. S.; Noh, J. H.; Jeon, N. J.; Kim, Y. C.; Ryu, S.; Seo, J.; Seok, S. I. High-performance

photovoltaic perovskite layers fabricated through intramolecular exchange. *Science* **2015**, *348* (6240), 1234–1237, DOI: 10.1126/science.aaa9272.

4) Zhou, H.; Chen, Q.; Li, G.; Luo, S.; Song, T.-B. B.; Duan, H.-S. S.; Hong, Z.; You, J.; Liu, Y.; Yang, Y. Interface engineering of highly efficient perovskite solar cells. *Science* **2014**, *345* (6196), 542–546, DOI: 10.1126/science.1254050.
5) Burschka, J.; Pellet, N.; Moon, S.-J. J.; Humphry-Baker, R.; Gao, P.; Nazeeruddin, M. K.; Grätzel, M. Sequential deposition as a route to high-performance perovskite-sensitized solar cells. *Nature* **2013**, *499* (7458), 316–319, DOI: 10.1038/nature12340, available at https://doi.org/10.1038/nature12340.
6) Tan, Z.-K. K.; Moghaddam, R. S.; Lai, M. L.; Docampo, P.; Higler, R.; Deschler, F.; Price, M.; Sadhanala, A.; Pazos, L. M.; Credgington, D.; Hanusch, F.; Bein, T.; Snaith, H. J.; Friend, R. H. Bright light-emitting diodes based on organometal halide perovskite. *Nature Nanotechnology* **2014**, *9* (9), 687–692, DOI: 10.1038/nnano.2014.149, available at https://doi.org/10.1038/nnano.2014.149.
7) Cho, H.; Jeong, S.-H. H.; Park, M.-H. H.; Kim, Y.-H. H.; Wolf, C.; Lee, C.-L.; Heo, J. H.; Sadhanala, A.; Myoung, N.; Yoo, S.; Im, S. H.; Friend, R. H.; Lee, T.-W. Overcoming the electroluminescence efficiency limitations of perovskite light-emitting diodes. *Science* **2015**, *350* (6265), 1222–1225, DOI: 10.1126/science.aad181.
8) Geerlings, P.; De Proft, F.; Langenaeker, W. Conceptual density functional theory. *Chemical reviews* **2003**, *103* (5), 1793–1874, DOI: 10.1021/cr990029p, available at https://doi.org/10.1021/cr990029p.
9) Kour, R.; Arya, S.; Verma, S.; Gupta, J.; Bandhoria, P.; Bharti, V.; Datt, R.; Gupta, V. Potential substitutes for replacement of lead in perovskite solar cells: a review. *Global Challenges* **2019**, *2019* (11), 1900050–1900050, DOI: 10.1002/gch2.201900050, available at https://doi.org/10.1002/gch2.201900050.
10) Zheng, Q.; Ji, Z.; Li, D. Theoretical studies on the effect of pressure on the electronic structure and optical properties of orthorhombic SmAlO3. *Optik* **2018**, *174*, 642–64, DOI: 10.1016/j.ijleo.2018.08.121, available at https://doi.org/10.1016/j.ijleo.2018.08.121.
11) Zeng, Z.; Xu, Y.; Zhang, Z.; Gao, Z.; Luo, M.; Yin, Z.; Zhang, C.; Xu, J.; Huang, B.; Luo, F.; Du, Y.; Yan, C. Rare-earth-containing perovskite nanomaterials: design, synthesis, properties and applications. *Chemical Society Reviews* **2020**, *49* (4), 1109–1143, DOI: 10.1039/C9CS00330D.
12) Ossila, 2015; available at https://www.ossila.com/pages/perovskites-and-perovskite-solar-cells-an-introduction.
13) Li, J.; Qiu, T. Synthesis and characterization of SmAlO3 dielectric material by citrate precursor method. *Journal of sol-gel science and technology Springer* **2012**, *61*, 112–118, DOI: 10.1007/s10971-011-2598-1, available at https://doi.org/10.1007/s10971-011-2598-1.
14) Iqbal, N. E.; Bashir, M. A DFT study of structural, electronic and optical properties of pristine and intrinsic vacancy defects containing barium zarconate (BaZrO3) using mBJ potential. *Physica Scripta* **2021**, *96*, 25807–25807, DOI: 10.1088/1402-4896/abd3c0, available at https://doi.org/10.1088/1402-4896/abd3c0.
15) Kohn, W.; Sham, L. J. Self-Consistent Equations Including Exchange and Correlation Effects. *Physical Review* **1965**, *140* (4A), A1133–A1138, DOI: 10.1103/PhysRev.140.A1133, available at https://doi.org/10.1103/PhysRev.140.A1133.
16) Blaha, P.; Schwarz, K.; Sorantin, P.; Trickey, S. B. Full-potential, linearized augmented plane wave programs for crystalline systems. *Computer Physics Communications* **1990**, *59*, 90187–90193, DOI: 10.1016/0010-4655(90)90187-6, available at https://doi.org/10.1016/0010-4655(90)90187-6.
17) Erum, N.; Iqbal, M. A.; Sagar, S.; Nabi, F. U. Effect of Hydrostatic pressure on structural, electronic, optical and mechanical properties of Lanthanum Oxide (La<sub>2</sub>O<sub>3</sub>). *Physica Scripta* **2021**, *96* (11), 115702–115702.
18) Lu, Q.; Zhang, H.-Y. Y.; Cheng, Y.; Chen, X.-R. R.; Ji, G.-F. F. Phase transition, elastic and electronic properties of topological insulator Sb2Te3 under pressure: First principle study. *Chinese Physics B* **2016**, *25* (2), 026401–026401, DOI: 10.1088/1674-1056/25/2/026401, available at https://doi.org/10.1088/1674-1056/25/2/026401.
19) Zhang, H.; Cheng, Y.; Tang, M.; Chen, X.; Ji, G. First-principles study of structural, elastic, electronic and thermodynamic properties of topological insulator Sb2Te3 under pressure. *Computational Materials Science* **2015**, *96*, 342–347, DOI: 10.1016/j.commatsci.2014.09.045, available at https://doi.org/10.1016/j.commatsci.2014.09.045.
20) Erum, N.; Iqbal, M. A.; Ashraf, F. Effect of hydrostatic pressure on structural and opto-electronic properties for barium based oxide perovskite. *Physica Scripta* **2022**, *97* (4), 045802–045802, DOI: 10.1088/1402-4896/ac5694, available at https://doi.org/10.1088/1402-4896/ac5694.
21) Erum, N.; Iqbal, M. A. Elastomechanical and Magneto-Optoelectronic Investigation of RbCoF3: An ab initio DFT Study. *Acta Physica Polonica A* **2020**, *138* (3), 509–517.
22) Fox, M. *Optical Properties of Solids*; Oxford University Press: New York, 2011.
23) Mavin, J.; Weber, In *Handbook of Optical Materials*; and others„ Ed.; CRC Press LLC, 2003.
24) Slater, J. C. The Ferromagnetism of Nickel. *Physical Review* **1936**, *49* (7), 537–545, DOI: 10.1103/PhysRev.49.537, available at https://doi.org/10.1103/PhysRev.49.537.